Endothelial cell invasion is controlled by dactylopodia

Ana Martins Figueiredo[a,1], Pedro Barbacena[a,1], Ana Russo[a], Silvia Vaccaro[a], Daniela Ramalho[a], Andreia Pena[a], Aida Pires Lima[a], Rita Rua Ferreira[a], Marta Alves Fidalgo[a], Fatima El-Marjou[b], Yulia Carvalho[a], Francisca Ferreira Vasconcelos[a], Ana-Maria Lennon-Duménil[c], Danijela Matic Vignjevic[b], and Claudio Areias Franco[a,d,2]

[a]Instituto de Medicina Molecular João Lobo Antunes, Faculdade de Medicina, Universidade de Lisboa, 1649-028 Lisboa, Portugal; [b]Institut Curie, Paris Sciences et Lettres Research University, CNRS UMR144, 75005 Paris, France; [c]Institut Curie, Paris Sciences et Lettres Research University, INSERM U932, 75005 Paris, France; and [d]Instituto de Histologia e Biologia do Desenvolvimento, Faculdade de Medicina, Universidade de Lisboa, 1649-028 Lisboa, Portugal

Edited by Janet Rossant, The Gairdner Foundation, Toronto, ON, Canada, and approved March 27, 2021 (received for review December 2, 2020)

Sprouting angiogenesis is fundamental for development and contributes to cancer, diabetic retinopathy, and cardiovascular diseases. Sprouting angiogenesis depends on the invasive properties of endothelial tip cells. However, there is very limited knowledge on how tip cells invade into tissues. Here, we show that endothelial tip cells use dactylopodia as the main cellular protrusion for invasion into nonvascular extracellular matrix. We show that dactylopodia and filopodia protrusions are balanced by myosin IIA (NMIIA) and actin-related protein 2/3 (Arp2/3) activity. Endothelial cell-autonomous ablation of NMIIA promotes excessive dactylopodia formation in detriment of filopodia. Conversely, endothelial cell-autonomous ablation of Arp2/3 prevents dactylopodia development and leads to excessive filopodia formation. We further show that NMIIA inhibits Rac1-dependent activation of Arp2/3 by regulating the maturation state of focal adhesions. Our discoveries establish a comprehensive model of how endothelial tip cells regulate its protrusive activity and will pave the way toward strategies to block invasive tip cells during sprouting angiogenesis.

angiogenesis | endothelial cells | invasion | actin | myosin

The formation of new blood vessels from preexisting ones—sprouting angiogenesis—is a fundamental process in health and disease (1, 2). Sprouting angiogenesis depends on the ability of a specialized endothelial cell (EC)—the tip cell—to invade and migrate into tissues (3), yet we still lack basic understanding of how endothelial tip cells migrate and invade into tissues. During three-dimensional cell migration, endothelial tip cells, as other mesenchymal-like cells such as fibroblasts and cancer cells, adopt a vast array of polarized membrane protrusions, which are essential for invasion and guidance (4–7). Membrane protrusions, such as lamellipodia and filopodia, are driven by actin dynamics (6, 8). Formin-dependent linear actin arrays promote filopodia formation, while actin-related protein 2/3 (Arp2/3) complex-dependent, dendritic actin arrays promote lamellipodia formation (6). In addition, nonmuscle myosin II (NNMII)-dependent contractility was shown to inhibit protrusions and to promote membrane blebbing, through cortical tension (9, 10), while a recent study showed that NNMIIA, a specific NNMII isoform, could also promote filopodia stability (11). The balance between these different filamentous actin networks and their regulators shapes the types of cellular protrusions formed and hence the mode of migration.

Vascular endothelial growth factor (VEGF) signaling is a master regulator of tip cell biology, and it was shown to regulate endothelial tip cell invasion and sprouting angiogenesis (1, 2, 12). CDC42 and RAC1, downstream of VEGF, are master regulators of endothelial tip cell membrane protrusions (13–15). VEGF also activates serum response factor (SRF), a transcription factor highly expressed by endothelial tip cells. Together with its cofactors myocardin-related transcription factors (MRTFs), SRF regulates endothelial invasive behavior by promoting filopodia formation (16–18). In addition, focal adhesions (FAs) are also crucial for EC migration and invasion, and deletion of integrin-linked kinase or integrin β1 (ITGB1) leads to severe sprouting angiogenesis defects and changes in tip cell protrusive activity (19, 20).

Despite their central role in tip cell invasion, it remains to be determined how actomyosin and its regulators affect cell shape and protrusive behavior and how different membrane protrusions influence EC migration in vivo. For instance, by using low doses of latrunculin B, a pharmacological inhibitor of actin polymerization, a recent report proposed that filopodia are dispensable for EC guidance and migration in zebrafish (21), generating controversy in the field.

Here, we investigated the specialized membrane protrusions on endothelial tip cells and their physiological relevance for EC invasion and angiogenesis in vivo and generated an integrative model of how endothelial tip cells invade into tissues.

Results

SRF/MRTFs activity was shown to regulate NNMII levels in ECs (16). ECs express mostly two isoforms of NNMII, NNMIIA and NNMIIB, which are coded by Myh9 and Myh10, respectively (betsholtzlab.org/VascularSingleCells/database.html) (22). To evaluate the function of NNMII in endothelial tip cells, we first investigated the location and expression levels of NNMIIA and NNMIIB. We first focused on NNMIIA. We found that endothelial tip cells express higher levels of NNMIIA than stalk cells, the cells juxtapose to tip cells that participate in the invading vascular sprout (Fig. 1 *A* and *B*, *SI Appendix*, Fig. S1 *A* and *B*, and Movies S1 and S2). We further confirmed these observations by imaging fluorescently tagged

Significance

In this report, we describe how endothelial cells, the cells lining the interior of blood vessels, invade into tissues to form new vessels through sprouting angiogenesis. We found that endothelial cells use a specific lamellipodia-related membrane protrusion for invasion, which we termed dactylopodia. These protrusions have a special morphology, originate from filopodia, are linked to membrane-ruffling activity, and are specialized in invading into avascular extracellular matrix. Our work lays the foundations for drug discovery targeting sprouting angiogenesis.

Author contributions: A.M.F., P.B., and C.A.F. designed research; A.M.F., P.B., A.R., S.V., D.R., A.P., A.P.L., R.R.F., M.A.F., Y.C., and C.A.F. performed research; F.E.-M., Y.C., A.-M.L.-D., D.M.V., and C.A.F. contributed new reagents/analytic tools; A.M.F., P.B., A.R., S.V., A.P.L., M.A.F., F.F.V., and C.A.F. analyzed data; and A.M.F., P.B., F.F.V., A.-M.L.-D., D.M.V., and C.A.F. wrote the paper.

The authors declare no competing interest.

This article is a PNAS Direct Submission.

[1]A.M.F and P.B. contributed equally to this work.

[2]To whom correspondence may be addressed. Email: cfranco@medicina.ulisboa.pt.

This article contains supporting information online at https://www.pnas.org/lookup/suppl/doi:10.1073/pnas.2023829118/-/DCSupplemental.

Published April 26, 2021.

NMIIA, using the Myh9-eGFP transgenic animals (*SI Appendix*, Fig. S2*A*) (23). In addition to higher expression, we found that NMIIA was enriched at the base of filopodia protrusions (Fig. 1 *A* and *C* and *SI Appendix*, Fig. S2 *B* and *C*). NMIIB followed a similar pattern to NMIIA. It is highly expressed by endothelial tip cells, and it is enriched at the base of filopodia (*SI Appendix*, Fig. S2*C*). This spatial distribution of NMII isoforms correlates with high levels of phospho-myosin light chain and filamentous actin (*SI Appendix*, Fig. S2 *B–D*). These results suggest that endothelial tip cells have higher levels of actomyosin contractility at their leading edges, in particular at the base of filopodia. To evaluate the function of NMIIA and NMIIB in ECs, we deleted Myh9 or Myh10 alone, or both simultaneously, using the PDGFB-CreERT2 line (24). Single deletion of Myh10 in ECs (NMIIB EC knockout [KO]) did not significantly affect retinal vascular morphogenesis, although we noticed a small decrease in the number of filopodia in endothelial tip cells (*SI Appendix*, Fig. S3 *A–C*). Efficient depletion of NMIIB was observed by immunofluorescence (*SI Appendix*, Fig. S3*B*). Single deletion of Myh9 (NMIIA EC-KO) showed a very distinct phenotype. NMIIA EC-KO retinas showed a mild decrease in radial expansion, an increase in vessel density, decreased proliferation, and an increase in the number of tip cells (Fig. 1 *D–F*). In accordance with a mild radial expansion phenotype, vascularization of the superficial in NMIIA EC-KO animals reached the retina margin by postnatal day 12 (P12) (*SI Appendix*, Fig. S4). Yet the most striking phenotype is a dramatic change in tip cell morphology (Fig. 1*E* and *SI Appendix*, Fig. S4*A*). NMIIA-deficient tip cells showed an abnormal branched morphology with extremely long and enlarged membrane protrusions and a severe decrease in filopodia number (Fig. 1*E* and *SI Appendix*, Fig. S5*A*). Remarkably, the absence of filopodia and enlarged membrane protrusions was tip cell specific, as ECs in nonsprouting areas showed numerous bona fide filopodia morphologically similar to wild-type (WT) control littermates, even if NMIIA-deficient ECs in the plexus show a trend to have a decreased number of filopodia (*SI Appendix*, Fig. S5 *B* and *C*). Immunofluorescence analysis confirmed the efficient depletion of NMIIA (Fig. 1*G*) and that the NMIIA EC-KO phenotype manifested even in the presence of high levels of NMIIB in tip cells (*SI Appendix*, Fig. S5*D*). Despite the notable changes in tip cell morphology, filamentous actin did not appear to be severely compromised with noticeable actin cables present in the cell cortex (Fig. 1*G*). Abrogation of both Myh9 and Myh10 led to an extremely severe phenotype, in which ECs at the sprouting front lacked filopodia and showed very elongated and slim membrane protrusions, likely caused by a complete disruption of actomyosin contractility (*SI Appendix*, Fig. S6 *A–C*). Altogether, these results revealed that NMIIA plays a fundamental role in the formation of tip cells' filopodia, which cannot be rescued by NMIIB. In addition, NMIIA and NMIIB, together, are essential to maintain EC shape. This is consistent with previous observations that both NMII isoforms play overlapping but also unique roles (23, 25–27).

The specific impairment of filopodia formation and the presence of long membrane protrusions in NMIIA-deficient tip cells, suggested that NMIIA plays an important role in the regulation on the type of membrane protrusions that tip cells produce (Fig. 1 *E* and *G* and *SI Appendix*, Fig. S5*A*). Thus, we decided to investigate the dynamics of membrane protrusions in endothelial tip cells in vivo. To do so, we established a protocol for live imaging of the mouse retina. Briefly, intact retinas are flat mounted using low-melting agarose and imaged shortly after retinal dissection on a multiphoton microscope (details in *Methods*). This protocol differs from previous protocols (28, 29), as it uses low-melting agarose which maintains retinal structure in a flat-mounted state that enables long-term (up to 6 h), high-resolution imaging using immersion objectives. Live imaging showed that WT endothelial tip cells have a high rate of filopodia formation (~0.6 filopodia/s) (Fig. 2 *A* and *B*, *SI Appendix*, Fig. S7 *A* and *B*, and Movies S3–S6). Surprisingly, live imaging of NMIIA-deficient retinas showed that tip cells were also able to protrude filopodia, albeit with significant altered dynamics (lower rate of initiation, lower extension speed, and duration of extension) (Fig. 2 *A* and *B*, *SI Appendix*, Fig. S7 *A* and *B*, and Movies S7–S11). Intriguingly, in both NMIIA WT and NMIIA EC-KO tip cells, we observed an unexpected membrane-ruffling activity at the filopodia membrane (Fig. 2 *A* and *B*, *SI Appendix*, Fig. S7 *A* and *B*, and Movies S7–S11). WT tip cells exhibited membrane ruffling both at filopodium's base and along filopodium's lateral membrane (Fig. 2 *A* and *B* and Movies S3–S6), yet ruffling activity was not a general feature of all filopodia. In our imaging conditions, only a small proportion of filopodia showed ruffling activity in their lifespan, and most of them extended and retracted without detectable ruffling activity. Moreover, when present, filopodium's ruffling was normally short lived (1 to 6 min). Ruffling activity at filopodium's base was associated with extension and enlargement of the cytoplasmic membrane (Fig. 2 *A* and *B* and *SI Appendix*, Fig. S7 *A* and *B*). Live imaging of NMIIA WT LifeAct-GFP retinas showed high and dynamic actin polymerization at the base of filopodia (*SI Appendix*, Fig. S7*C* and Movies S12 and S13), suggesting that membrane ruffling is driven by actin polymerization. In contrast to NMIIA WT tip cells, membrane ruffling in NMIIA EC-KO tip cells was more persistent and generally led to the conversion of filopodia into long membrane protrusions, similar to the ones observed in fixed samples (Fig. 2*A*, *SI Appendix*, Fig. S7*A*, and Movies S7–S11). Thus, our live-imaging observations indicate that long membrane protrusions in NMIIA-deficient tip cells are originated from altered filopodia dynamics through excessive actin-dependent membrane ruffling. Moreover, they suggest that one key function of NMIIA in tip cells is to negatively regulate the formation of such long protrusions.

Given that NMIIA WT tip cells also showed substantial filopodia membrane ruffling (Movies S4–S6), we reasoned that the formation of long membrane protrusions might be a particular feature of WT tip cells that become overrepresented in NMIIA EC-KO. Indeed, careful analysis of WT tip cells showed similar morphological membrane protrusions, comparable to the prominent ones observed in NMIIA EC-KO tip cells, yet their frequency and size were much reduced (Fig. 2 *C–E* and *SI Appendix*, Fig. S8*A*). In WT tip cells, these membrane protrusions were characterized by a mean length of ~20 μm (ranging from ~5 to ~33 μm) and a mean width of ~2 μm (ranging from ~0.7 to ~5 μm) (Fig. 2*E*), enriched in actin and NMIIA, and from which numerous filopodia emanated (Fig. 2 *C* and *D* and *SI Appendix*, Fig. S8*B*). Given their morphology (finger-like protrusions), originated from filopodia and linked to membrane-ruffling activity, we named these naturally occurring protrusions as dactylopodia. Interestingly, the presence of dactylopodia correlated with regions where endothelial tip cells contacted with nonvascular extracellular matrices (ECM), highlighted by decreased staining of the vascular basement membrane marker collagen IV (Fig. 2*F* and *SI Appendix*, Fig. S8*C*). Moreover, dactylopodia were associated with increased levels of active ITGB1, a marker for matrix-bound FAs (*SI Appendix*, Fig. S8*C*). Dactylopodia in NMIIA-deficient ECs also correlated with sites of contact with nonvascular extracellular matrix and with activated ITGB1; however, its expression pattern appeared to be more diffused along dactylopodia and not enriched at the base of filopodia, as in WT cells (*SI Appendix*, Fig. S8*C*). Altogether, these data suggest that dactylopodia are endothelial tip cell–specific protrusions derived from filopodia that might play roles in invasion and migration into nonvascular ECM.

Next, we investigated the mechanism driving dactylopodia formation in ECs. Actin-based membrane ruffling is known to rely on Arp2/3-dependent, dendritic actin networks (6). To confirm if Arp2/3 is involved in dactylopodia formation, we specifically deleted Arpc4, a structurally essential component of the Arp2/3 complex (5, 30), in ECs in vivo. Deletion of Arpc4 in ECs, Arpc4 EC-KO, led to a very prominent vascular phenotype. ECs without a functional

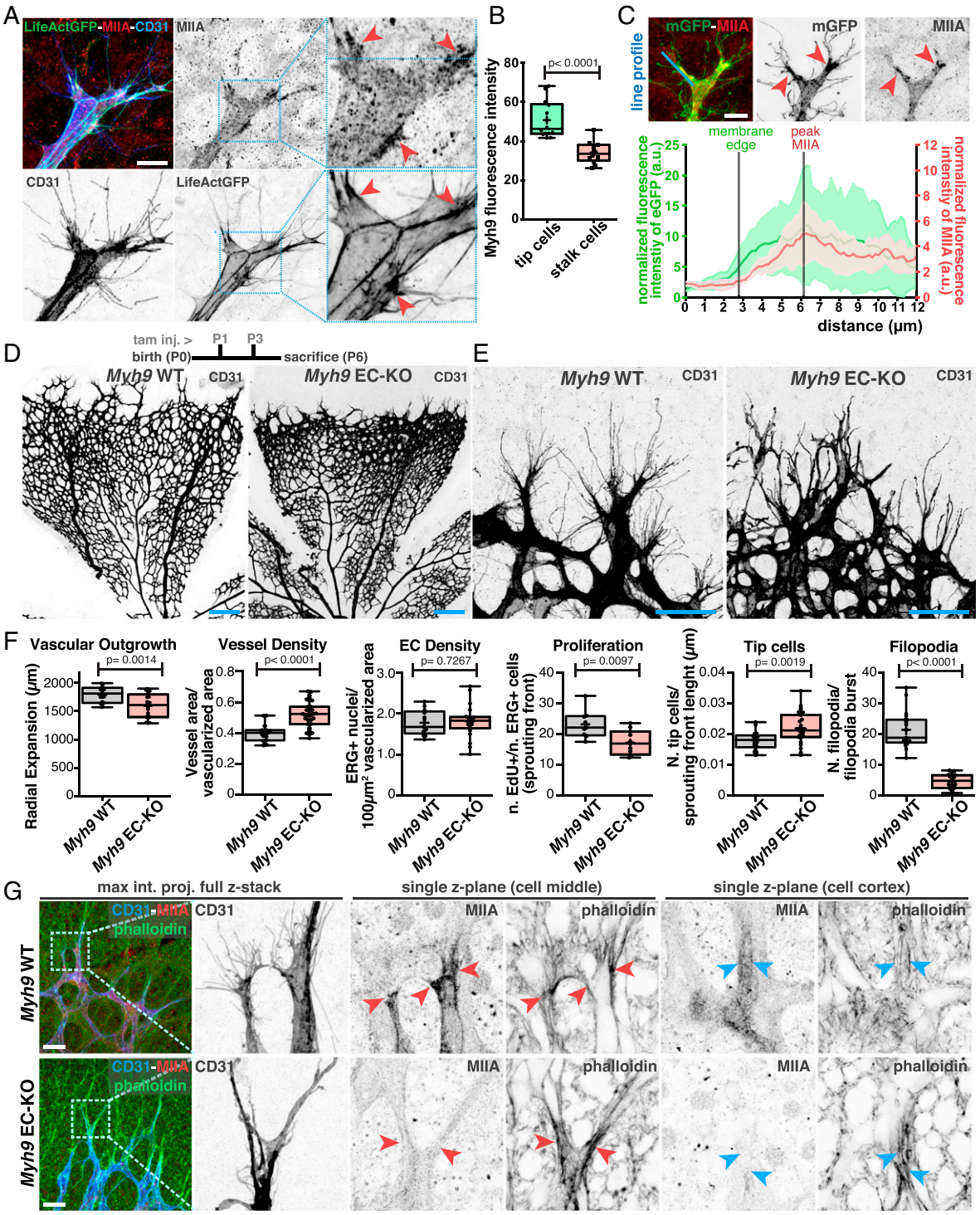

Fig. 1. (*A*) Representative images of tip cells from LifeAct-GFP mouse retinas labeled for NMIIA (red), actin (green), and CD31 (blue). Red arrowheads point to sites enriched in NMIIA at the base of filopodia. (Scale bar, 20 μm.) (*B*) Box plot of Myh9 fluorescence intensity between tip and stalk cells from *PDGFB-iCRE::mTmG* mouse retinas (n = 14 tip cells and n = 12 stalk cells). *P* value from unpaired Student's *t* test. (*C*, *Upper*) Representative image in which red arrowheads point to sites enriched in NMIIA at the base of filopodia. (Scale bar, 20 μm.) (*Bottom*) Graph of the normalized line-scan fluorescence intensity profile (blue line) for NMIIA and mGFP signals from the endothelial tip cell's leading edge (n = 6 endothelial tip cells). Lines represent the beginning of the plasma membrane and peak of NMIIA levels. The NMIIA signal shows a peak of intensity subsequent to the beginning of the filopodia burst. (*D*, *Upper*) Timeline of tamoxifen injection (tam. inj.) and age killed of mouse pups. The representative images of mouse retinas from *Myh9* WT and *Myh9* EC-KO are labeled for CD31. (Scale bar, 250 μm.) (*E*) Representative images of tip cells and filopodia in the angiogenic sprouting front of mouse retinas from *Myh9* WT and *Myh9* EC-KO labeled for CD31. (Scale bar, 50 μm.) (*F*) Box plots of vascular outgrowth, vessel density, EC density, EC proliferation, number of tip cells, and number of filopodia per filopodia burst in *Myh9* WT (n = 19 retinas) and *Myh9* EC-KO (n = 24 retinas) mouse retinas. *P* value from unpaired Student's *t* test. (*G*, *Left*) High-magnification images of tip cells labeled for CD31 (blue), F-actin (green), and NMIIA (red) from *Myh9* WT and *Myh9* EC-KO. (*Right*) Higher-magnification images from delineated regions in Left for single z-plane of tip cells in two different planes. Red arrowheads point toward leading edges of tip cells; blue arrowheads point toward cortical actin cables in tip cells. (Scale bar, 50 μm.)

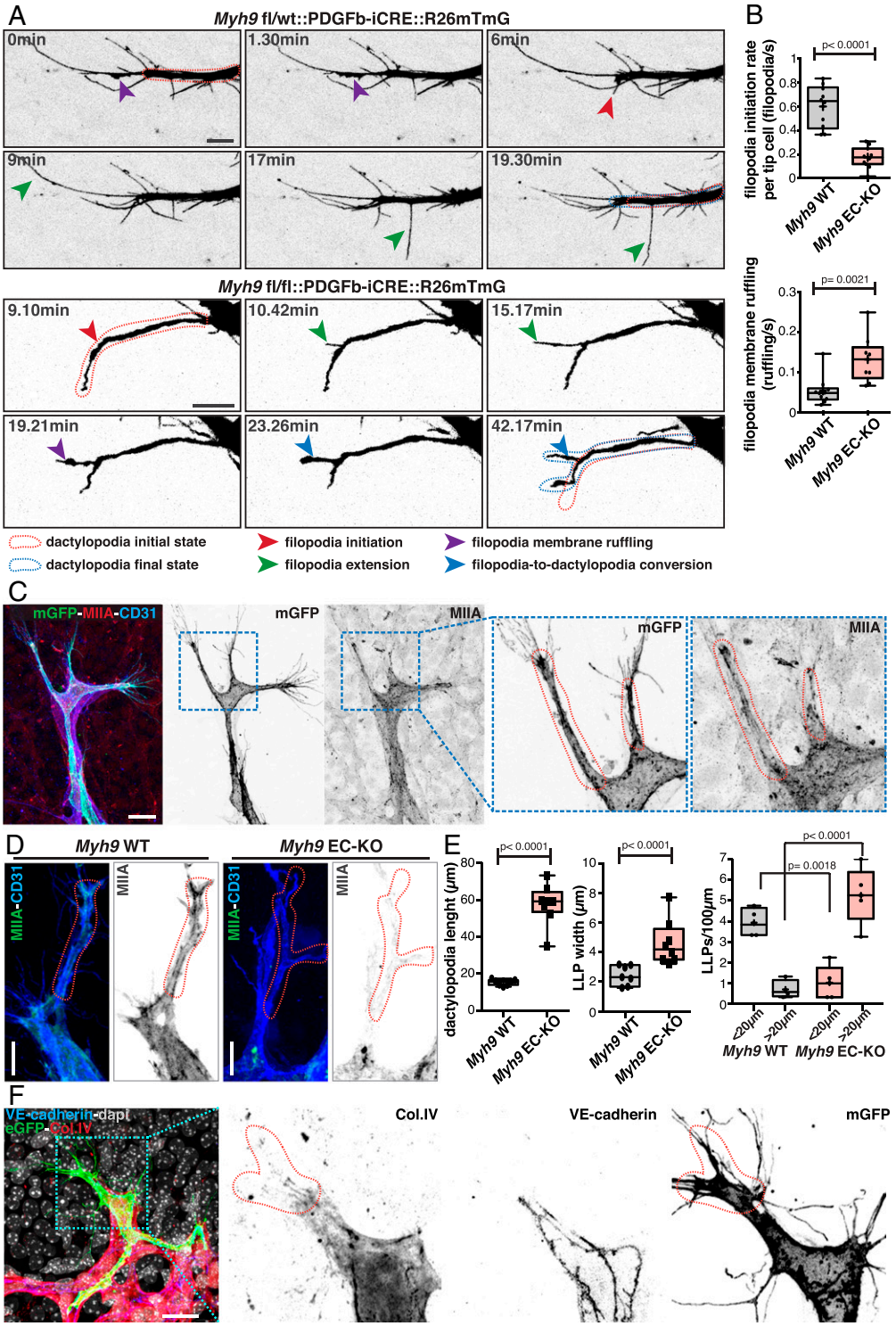

Fig. 2. (*A*) Time-course still images of dactylopodia and filopodia dynamics in *Myh9 fl/wt::PDGFB-iCRE::R26mTmG* and *Myh9fl/fl::PDGFB-iCRE::R26mTmG* mouse retinas. Red dashed line contour represents dactylopodia initial state. Blue dashed line contour represents dactylopodia final state. Red arrow indicates filopodia initiation; green arrow indicates filopodia extension; purple arrow indicates filopodia membrane ruffling; and blue arrow indicates filopodia-to-dactylopodia conversion. (Scale bar, 10 μm.) (*B*) Box plots of filopodia initiation rate per tip cell (filopodia/second) (*Myh9* WT n = 10 tip cells and *Myh9* EC-KO n = 11 tip cells) and filopodia membrane ruffling (ruffling/second) in *Myh9* WT (*Myh9* WT n = 10 filopodia) and *Myh9* EC-KO (*Myh9* EC-KO n = 9 filopodia) mouse retinas. *P* value from unpaired Student's *t* test. (*C*) Representative images of a tip cell from a *PDGFb-iCre::R26mTmG* mouse retina labeled for NMIIA (red), cell membrane (green), and CD31 (blue), highlighting dactylopodia in tip cells (red dashed line) with numerous filopodia in their extremity. (Scale bar, 20 μm.) (*D*) Representative images of tip cells and dactylopodia from *Myh9* WT and *Myh9* EC-KO mouse retinas labeled for NMIIA (green) and CD31 (blue). (Scale bar, 10 μm.) Red dashed line contours dactylopodia. (*E*) Box plots of number of dactylopodia (<20 μm or >20 μm) in *Myh9* WT (n = 4 retinas) and *Myh9* EC-KO mouse retinas (n = 5 retinas) and dactylopodium width and length in *Myh9* WT (n = 7 retinas) and *Myh9* EC-KO mouse retinas (n = 8 retinas). *P* value from unpaired Student's *t* test. (*F*) Representative images of dactylopodia in tip cells from a *PDGFb-iCRE::R26mTmG* (green) P6 mouse retina labeled for vascular endothelial–cadherin (blue), Col.IV (red), and nuclei (DAPI, gray). (Scale bar, 20 μm.) Red dashed line contours dactylopodia.

Arp2/3 complex were unable to invade into avascular areas, leading to a dramatic reduction in radial expansion at P6 (Fig. 3 *A*–*C*). Higher magnification of tip cells demonstrated that Arpc4-deficient cells had a reduced number of dactylopodia, which correlated with an increase in the number and length of filopodia (Fig. 3 *B*, *D*, and *E*). Strikingly, Arpc4 EC-KO phenotype inversely mirrors NMIIA EC-KO phenotype in terms of tip cells' filopodia and dactylopodia number and morphology (compare Figs. 1 *E* and *F* and 3 *B* and *C*). Yet Arp2/3 deficiency did not alter NMIIA distribution in endothelial tip cells (Fig. 3*D*). Analysis of P12 retinas showed that radial expansion was completely abrogated, as radial outgrowth was mostly at the same distance from the optic nerve as in P6 retinas (*SI Appendix*, Fig. S9*A*). Altogether, we conclude that dactylopodia are formed by Arp2/3-dependent actin polymerization and that endothelial tip cell invasiveness is entirely determined by Arp2/3 activity. Moreover, it proves that the presence of filopodia is insufficient for tip cell invasion.

Next, we investigated how the balance between filopodia and dactylopodia in endothelial tip cells is established. Remarkably, NMIIA KO phenotype was characterized by a loss of filopodia and a gain in dactylopodia, while Arpc4 EC-KO displayed excessive filopodia and a reduced number of dactylopodia. Moreover, we showed that dactylopodia originated from filopodia. Thus, we hypothesized that NMIIA could balance the ability of tip cells to form filopodia over dactylopodia by regulating Arp2/3 complex activity. A prediction from this model is that inhibition of the Arp2/3 complex in NMIIA-deficient cells should rescue the ability of ECs to produce filopodia. To test this hypothesis, we turned to in vitro human umbilical vein EC (HUVEC) cultures. ECs' growth on glass or plastic did not show the ability to form long filopodia. However, when seeded on top of fibroblast monolayers, HUVECs acquired this capacity (31). However, in both in vitro conditions, HUVECs did not display protrusions similar to dactylopodia but rather standard lamellipodia. DMSO-treated or CK666-treated (a specific inhibitor of Arp2/3) cells have a similar number of filopodia in normal conditions. In contrast, blebbistatin (BBS), an inhibitor of NMII activity, abrogated filopodia formation. Remarkably, filopodia formation in BBS-treated cells was partially rescued by cotreatment with CK666 (*SI Appendix*, Fig. S10 *A* and *B*). These results were further confirmed by small interfering RNA-mediated knockdown of NMIIA and Arp2/3 complex (*SI Appendix*, Fig. S10 *C* and *D*). To further confirm these observations, we used an optogenetic tool that allows timed and local activation of Cdc42 (32), the main regulator of EC protrusions in vivo and in vitro (13). We observed that, in DMSO-treated conditions, Cdc42 activation led to high lamellipodia activity and few filopodia, which was reverted by an inhibitor of Arp2/3 (CK666) (Fig. 4 *A* and *B* and Movies S14 and S15). In contrast, BBS treatment abrogated filopodia formation (Fig. 4 *A* and *B* and Movie S16). The capacity of forming filopodia in BBS-treated cells was restored by cotreatment with CK666 (Fig. 4 *A* and *B* and Movie S17), supporting the hypothesis that NMII activity promotes filopodia formation by limiting the activation of Arp2/3. To verify if NMIIA EC-KO leads to a lack of filopodia and an excess of dactylopodia due to unrestrained Arp2/3 activity in vivo, we generated a double loss of function of both Arp2/3 and NMIIA by crossing NMIIA EC-KO and Arpc4 EC-KO mice. Overall, Arpc4::NMIIA EC double KO mice showed a phenotype very similar to Arpc4 EC-KO, with a strong reduction in radial expansion and compaction at the vascular front (Fig. 4 *C* and *D*). Yet abrogation of Arp2/3 rescued filopodia formation in NMIIA-deficient ECs in vivo (Fig. 4 *E* and *F* and *SI Appendix*, Fig. S9*B*). Altogether, these results demonstrate that NMIIA enables filopodia stability by restricting Arp2/3 activation in endothelial tip cells in vivo.

We next investigated the mechanism by which NMIIA limits Arp2/3 activity. Arp2/3 is activated by WASP/WAVE complexes downstream of the Rho GTPases, Rac1 and Cdc42 (33). A common trigger for Rac1/Cdc42 activation and migration is signaling from immature FAs at the leading edge of cells (33, 34). Our observations showed that Arp2/3-dependent dactylopodia correlated with local invasion into extravascular matrices (Fig. 2*F* and *SI Appendix*, Fig. S7), suggesting that integrin-mediated signaling could activate Arp2/3 when engaging with extravascular matrices. In accordance, ITGB1 EC-KO shows striking similarities with Arpc4 EC-KO, including excessive and longer filopodia formation, blunted sprouting front (reminiscent of a lack of dactylopodia), and severely reduced invasion to deeper layers (20). Moreover, it is well established that NMII-dependent activity promotes maturation of integrin adhesions (35). Thus, we hypothesized that Fas could be a platform promoting the cross-talk between NMIIA and Arp2/3 complex at the leading edge of tip cells. To evaluate the state of Fas, we analyzed integrins (ITGA5 and activated ITGB1) and phosphorylated paxillin (pPAX, a marker for more mature FAs). WT tip cells showed high levels of pPAX and activated ITGB1 at the base of filopodia and in dactylopodia but also an enrichment of both ITGA5 and ITGB1 (Fig. 5*A* and *SI Appendix*, Fig. S11 *A* and *B*). NMIIA-deficient tip cells showed a significant reduction of pPAX, and signals for both ITGA5 and activated ITGB1 were diffused all over dactylopodia when compared to WT tip cells (Fig. 5 *A* and *B* and *SI Appendix*, Fig. S11 *A* and *B*). These observations suggest that the inhibition of NMIIA leads to significant differences in integrin location and activation state. Similar results were observed in ECs in vitro. BBS-mediated inhibition of NMII in HUVEC fibroblasts cocultures led to a strong decrease in the number of mature fibrillar Fas and a strong decrease in pPAX, both at immunofluorescence and Western blot level, while CK666 treatment did not modify levels of pPAX (Fig. 5 *C* and *D* and *SI Appendix*, Fig. S12 *A*–*C*), which correlates with a decrease in the number of filopodia (*SI Appendix*, Fig. S10). Our results are suggestive of a mechanism in which immature/nascent adhesions would activate Arp2/3, and NMIIA inhibits this signaling axis by promoting maturation of Fas, as previously reported (35, 36). We next assessed if BBS treatment would promote activation of Rac1, a major positive regulator of Arp2/3 in ECs downstream of integrin signaling. We observed that BBS treatment increased the levels of Rac1-GTP, the active form of Rac1, when compared to DMSO treatment (Fig. 5*E*). Accordingly, inhibition of Rac1 activation with NSC23766 led to a rescue of filopodia formation in BBS-treated cells (Fig. 5*G* and *SI Appendix*, Fig. S13). Tiam1, DOCK180, and Arhgef7/β-PIX were previously implicated in Rac1 activation downstream of integrins (37). In addition, previous work showed that NMIIA inhibits β-PIX recruitment to and activation by FAs (36). Thus, we tested if knockdown of β-PIX could rescue filopodia formation in BBS-treated cells. Indeed, silencing of β-PIX (*SI Appendix*, Fig. S14*A*) led to a partial rescue in filopodia number in BBS-treated ECs (Fig. 5 *H* and *I* and *SI Appendix*, Fig. S14*B*). Taken together, these results suggest that NMIIA balances dactylopodia and filopodia formation by promoting FA maturation and thereby limiting Arp2/3 activation through inhibition of Rac1 activation downstream of integrin β-PIX in nascent adhesions.

Discussion

Deciphering the mechanisms used by ECs to migrate and invade is essential to understand sprouting angiogenesis and to develop novel anti-angiogenic therapies. Altogether, these results demonstrate 1) that Arp2/3 activity is necessary for endothelial tip cell invasiveness and formation of proinvasive dactylopodia; 2) that dactylopodia derive from filopodia; 3) that filopodia are not required for tip cell migration; and 4) that NMIIA enables filopodia stability by restricting Arp2/3 activation in endothelial tip cells in vivo. We found that invasiveness of endothelial tip cells during angiogenesis in vivo depends on the formation of specific Arp2/3-dependent protrusions, the dactylopodia. We found that dactylopodia are derived from filopodia at sites in contact

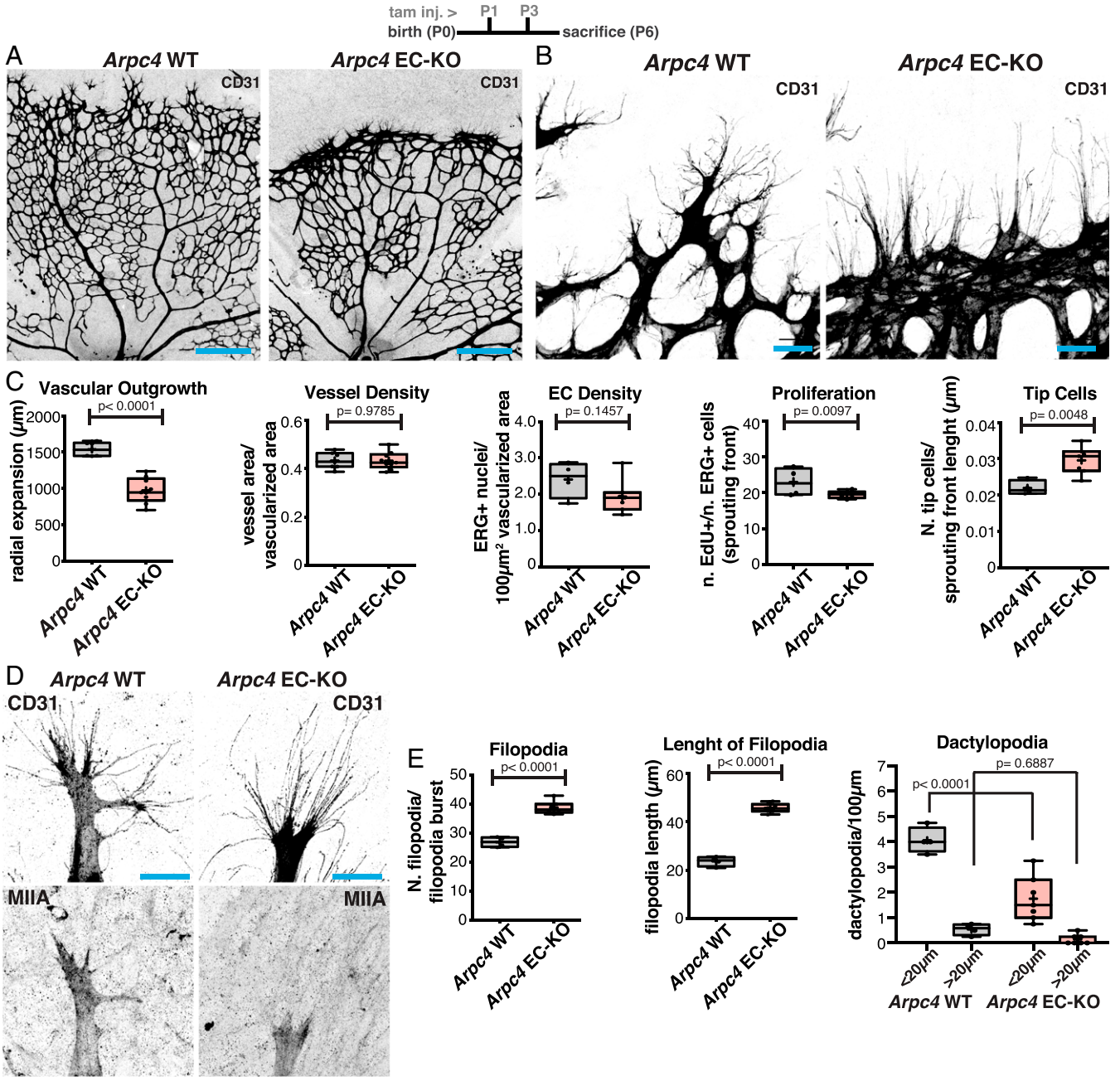

Fig. 3. (*A*) Representative images of mouse retinas from *Arpc4* WT and *Arpc4* EC-KO labeled for CD31. (Scale bar, 250 μm.) Please note that images were generated by tiling multiple fields of view, and that imperfect tiling generated misalignments between fields of view, which can be seen in the images. (*B*) Representative images of tip cells and filopodia in the angiogenic sprouting front of mouse retinas from *Arpc4* WT and *Arpc4* EC-KO labeled for CD31. (Scale bar, 50 μm.) (*C*) Box plots of vascular outgrowth, vessel density, EC density, EC proliferation, and number of tip cells per sprouting front length (micrometer) in *Arpc4* WT (n = 7 retinas) and *Arpc4* EC-KO (n = 9 retinas) mouse retinas. *P* values from unpaired Student's *t* test. (*D*) Representative images of tip cells from *Arpc4* WT and *Arpc4* EC-KO mouse retinas labeled for CD31 and NMIIA. (Scale bar, 20 μm.) (*E*) Box plots of number of filopodia per filopodia burst, length of filopodia (micrometer), and number of dactylopodia per 100 μm (<20 μm or >20 μm) in *Arcp4* WT (n = 4 retinas) and *Arpc4* EC-KO (n = 7 retinas) mouse retinas. *P* values from unpaired Student's *t* test.

with nonvascular extracellular matrix. Our findings also support the idea that filopodia are not per se sufficient for EC invasion and migration, as previously reported (21). Yet filopodia play a regulatory role as they serve as dactylopodia precursors. Interestingly, our live-imaging analysis showed that only a very small number of filopodia showed membrane-ruffling activity, and WT tip cells present an excess number of filopodia (~30) over dactylopodia (~4). Thus, the mechanisms allowing dactylopodia formation must be tightly regulated.

Previous studies have highlighted that Arp2/3 and formins compete with each other to regulate the organization of filamentous actin and to dictate the type of cellular protrusions (38, 39). Remarkably, we show that NMIIA balances the relative proportion of two types of cellular protrusions, favoring filopodia over dactylopodia, a lamellipodia-like structure. This is rather surprising as increased contractility is generally inversely correlated with protrusive activity, as shown in several different models (9, 10). Moreover, we discovered that NMIIA balances the protrusive activity of tip cells

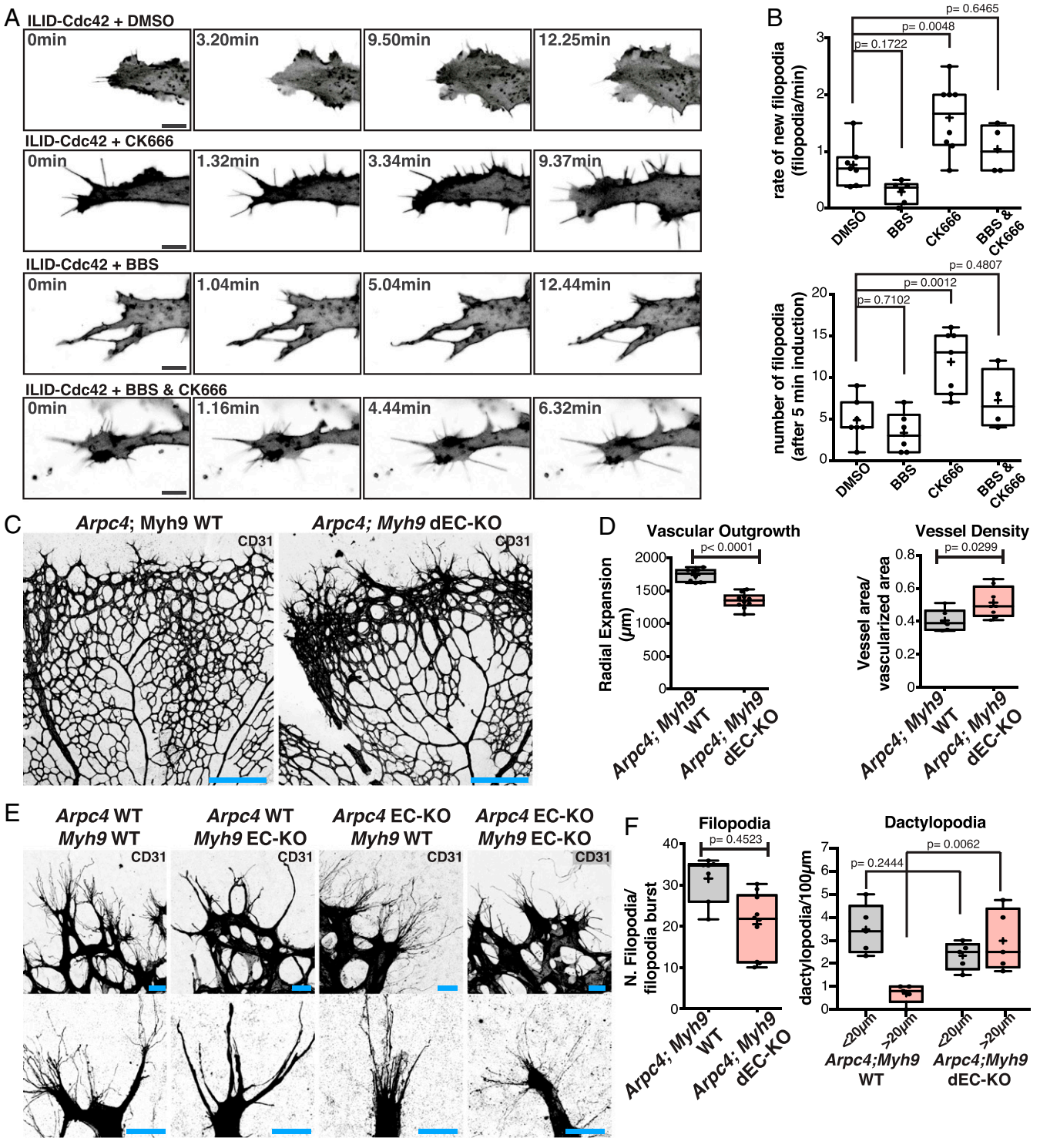

Fig. 4. (*A*) Representative images of HUVECs expressing an optogenetic activator of Cdc42 (ILID) in DMSO, BBS, CK666, and BBS + CK666 conditions. (Scale bar, 10 μm.) (*B*) Box plots of rate of new filopodia and total number of filopodia in different conditions (DMSO n = 7 cells; BBS n = 6 cells; CK666 n = 8 cells; and BBS + CK666 n = 4 cells). *P* values from unpaired ANOVA test. (*C*) Representative images of mouse retinas from *Arpc4;Myh9* WT and *Arpc4;Myh9* dEC-KO mouse retinas labeled for CD31. (Scale bar, 250 μm.) (*D*) Box plot of vascular outgrowth and vessel density in *Arpc4;Myh9* WT (n = 8 retinas) and *Arpc4;Myh9* dEC-KO (n = 10 retinas) mouse retinas. *P* values from unpaired Student's *t* test. (*E*) Representative images of tip cells and filopodia/dactylopodia from *Arpc4;Myh9* WT *Arpc4* EC-KO, *Myh9* EC-KO, and *Arpc4;Myh9* dEC-KO mouse retinas labeled for CD31 (gray). (Scale bar, 20 μm.) (*F*) Box plots of number of filopodia per filopodia burst and number of dactylopodia (<20 μm or >20 μm) in *Arpc4;Myh9* WT (n = 5 retinas) and *Arpc4;Myh9* dEC-KO mouse retinas (n = 5 retinas). *P* value from unpaired Student's *t* test.

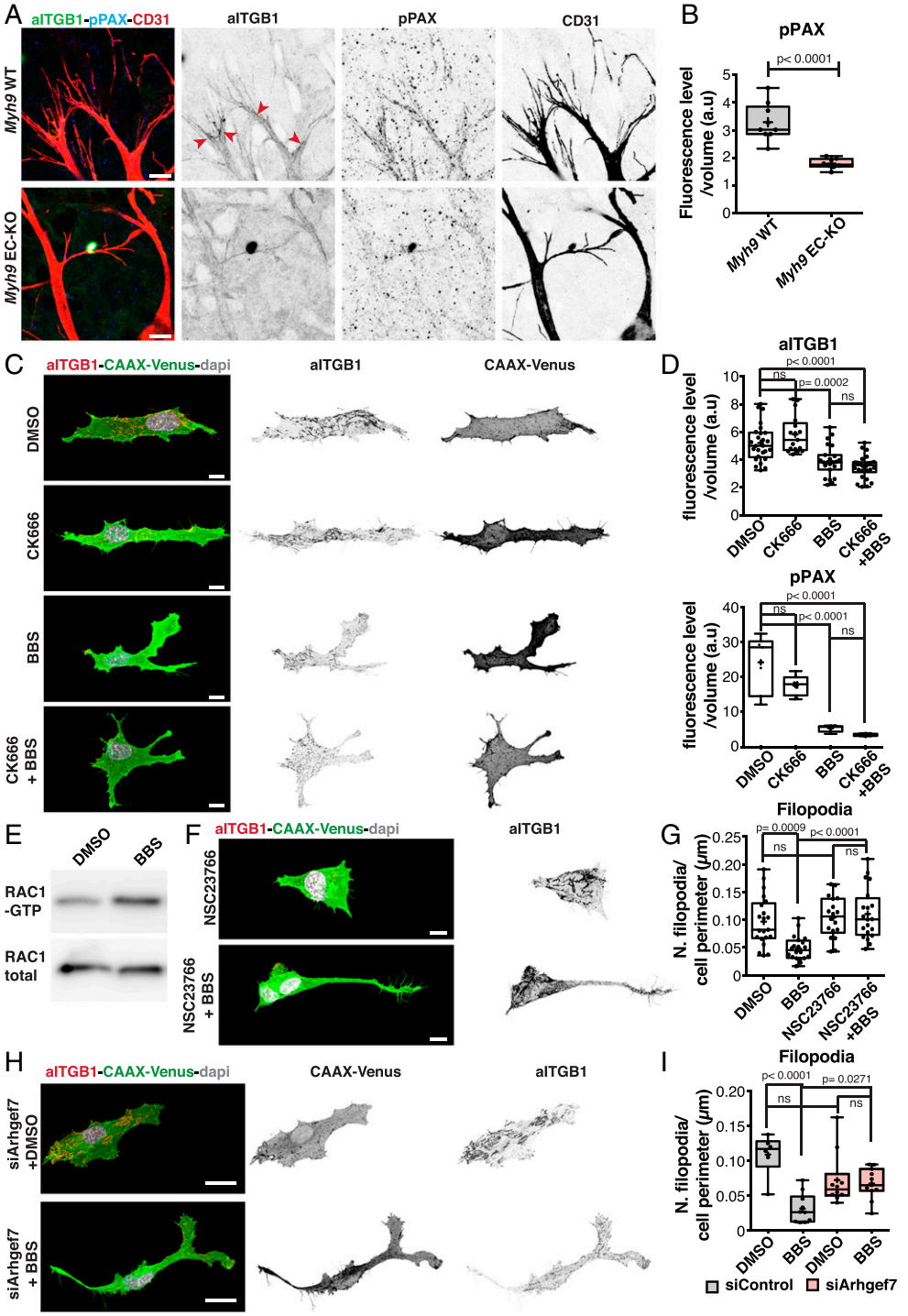

Fig. 5. (*A*) Representative images of tip cells from *Myh9* WT and *Myh9* EC-KO mouse retinas labeled for pPax Y118 (blue), activated ITGB1 (aITGB1, green), and CD31 (red). (Scale bar, 10 μm.) Red arrowheads point to sites enriched in aITGB1 and pPAX at the base of filopodia in *Myh9* WT tip cells, which is absent or more homogenously distributed along dactylopodia of *Myh9* EC-KO tip cells. (Scale bar, 20 μm.) (*B*) Box plot of pPax fluorescence in tip cells from *Myh9* WT (n = 9 retinas) and *Myh9* EC-KO (n = 8 retinas) mouse retinas. *P* value from unpaired Student's *t* test. (*C*) Representative images of HUVECs expressing CAAX-Venus at the cell membrane in DMSO, BBS, CK666, and BBS + CK666 conditions. HUVECs are labeled for aITGB1 (red), cell membrane (CAAX-Venus, green), and nuclei (DAPI, gray). (Scale bar, 10 μm.) (*D*) Box plots of pPax fluorescence intensity and aITGB1 fluorescence intensity in HUVECs expressing CAAX-Venus at the cell membrane in DMSO (n = 20 cells), BBS (n = 15 cells), CK666 (n = 24 cells), and BBS + CK666 (n = 13 cells) conditions. *P* values from one-way ANOVA. (*E*) Western blot analysis of levels of active GTP-bound Rac1 and total Rac1 in DMSO- or BBS-treated HUVECs. (*F*) Representative images of HUVECs expressing CAAX-Venus at the cell membrane in NSC23766 and NSC23766 + BBS conditions. HUVECs are labeled for aITGB1 (red), cell membrane (CAAX-Venus, green), and nuclei (DAPI, gray). (Scale bar, 10 μm.) (*G*) Box plot of filopodia number in DMSO (n = 21 cells), BBS (n = 20 cells), NSC23766 (n = 18 cells), and NSC23766 + BBS (n = 20 cells). *P* values from one-way ANOVA. (*H*) Representative images of HUVECs expressing CAAX-Venus at the cell membrane in siArhgef7 HUVECs treated with DMSO or BBS. HUVECs are labeled for aITGB1 (red), cell membrane (CAAX-Venus, green), and nuclei (DAPI, gray). (Scale bar, 10 μm.) (*I*) Box plot of filopodia number in siControl and siArhgef7 HUVECs treated with DMSO (n = 6 cells in siControl and 10 in siArhgef7) or BBS (n = 10 cells in siControl and 11 in siArhgef7). *P* values from one-way ANOVA.

by limiting Arp2/3 activation through actomyosin contractility-induced maturation of FAs. Notably, this effect was restricted to NMIIA and not NMIIB, in agreement with reports demonstrating that NMII isoforms have unique roles (23, 25–27). Recently, Ma et al. have also revealed the importance of NMIIA and NMIIB in sprouting angiogenesis during embryonic development (40). While the relative importance of each NMII isoform for a correct development of the vascular network is consistent with our observations, the effects of NMIIA deletion on cortical stability models was not consistent with our in vivo live-imaging results. Instead of an excess of cortical protrusions (filopodia and dactylopodia), we observed a net decrease in the overall number of cortical protrusions. Moreover, no blebbing behavior was observed, in contrast with observations in Ma et al. (40). These differences may be explained by the different models used for live imaging in the two studies, in vitro embryoid body sprouting assays in Ma et al. and our ex vivo assays. This highlights the specific differences and adaptive mechanisms in cell behavior from in vitro and in vivo conditions.

Based on this study and on previous reports, we propose an integrative view on the mechanisms regulating endothelial tip cell's invasive behavior: VEGFA controls formins, by directly regulating Cdc42 activity (13, 14) and NMIIA, via SRF transcriptional activity (16). This fosters actomyosin contractility and protrusive activity in endothelial tip cells. Cdc42/formin-dependent filopodia activity will engage with extravascular matrices, activating integrin signaling at the base and within filopodia, which promotes Arp2/3 activity downstream of a β-PIX/Rac1 pathway. NMIIA positively regulates the maturation state of FAs, which negatively regulates the β-PIX/Rac1 pathway and thus prevents excessive Arp2/3 activation. Loss of NMIIA activity leads to overactivation of Arp2/3 and unrestrained conversion of filopodia into dactylopodia. Loss of Arp2/3 activity abrogates dactylopodia formation and thus inhibits cell migration and invasion (*SI Appendix*, Fig. S15). Excessive filopodia formation in Arp2/3-deficient endothelium may be explained by the previously documented competition between actin nucleators (41). Within this model, an outstanding question relates to the mechanism of local control of NMIIA activity that licenses dactylopodium formation. We can speculate that filopodia-dependent signaling (engagement with local guidance cues and extravascular matrix components or cells) would trigger inhibition of NMIIA at the base of filopodia, leading to Arp2/3 activation and dactylopodia formation. Filopodia have been shown to produce pulling forces on the extravascular matrix, a propriety related to NMIIA activity (11), which could be related to dactylopodia formation. Exploration of this molecular cross-talk might provide therapeutic opportunities to sprouting angiogenesis, based on the ability to block invasion of endothelial tip cells.

Methods

Mice and Treatments. In this study, we used the following mouse strains: *Myh9* floxed (42); *Myh10* floxed (43); *Arpc4* floxed (30); LifeAct-GFP (44); R26mTmG (45); Myh9-GFP (46); and *Pdgfb*-iCreERT2 (24). Intercrosses between the different mouse strains generated new double and triple transgenic mouse strains. As controls, Cre-negative littermates were used in all experiments. Both males and females were used without distinction. Tamoxifen (Sigma) was injected intraperitoneally (20 μL/g of 1 mg/mL solution) at P1 and P3 before eyes were collected either at P6 and P12 or injected at P4 and P5 and collected at P12, as described previously (47). Additional details about mouse models, as well as all other materials and methods, are described in detail in *SI Appendix*.

Data Availability. All study data are included in the article and/or supporting information.

ACKNOWLEDGMENTS. We thank Clare M. Waterman, Robert Fischer, Robert Adelstein, and Xuefei Ma (National Heart, Lung, and Blood Institute) for discussion and technical support and João Barata, Edgar Gomes (Instituto de Medicina Molecular), and Michael Potente (Max Planck Institute for Heart and Lung Research) for critical review of the manuscript. We thank all members of the Vascular Morphogenesis Laboratory for helpful discussions and critical reading of the manuscript. C.A.F. was supported by a European Research Council starting grant (679368), the European Union H2020-TWINN-2015—Twinning (692322), the Fundação para a Ciência e a Tecnologia funding (grants IF/00412/2012, EXPL/BEX-BCM/2258/2013, PTDC/MED-PAT/31639/2017, and PTDC/BIA-CEL/32180/2017 and fellowships CEECIND/04251/2017 and CEECIND/02589/2018), and a grant from the Fondation Leducq (17CVD03).

1. H. G. Augustin, G. Y. Koh, Organotypic vasculature: From descriptive heterogeneity to functional pathophysiology. *Science* **357**, eaal2379 (2017).
2. M. Potente, T. Mäkinen, Vascular heterogeneity and specialization in development and disease. *Nat. Rev. Mol. Cell Biol.* **18**, 477–494 (2017).
3. H. Gerhardt *et al*., VEGF guides angiogenic sprouting utilizing endothelial tip cell filopodia. *J. Cell Biol.* **161**, 1163–1177 (2003).
4. G. Jacquemet, H. Hamidi, J. Ivaska, Filopodia in cell adhesion, 3D migration and cancer cell invasion. *Curr. Opin. Cell Biol.* **36**, 23–31 (2015). Correction in: *Curr. Opin. Cell Biol.* **37**, 119 (2015).
5. T. D. Pollard, Actin and actin-binding proteins. *Cold Spring Harb. Perspect. Biol.* **8**, a018226 (2016).
6. K. Rottner, M. Schaks, Assembling actin filaments for protrusion. *Curr. Opin. Cell Biol.* **56**, 53–63 (2019).
7. K. M. Yamada, M. Sixt, Mechanisms of 3D cell migration. *Nat. Rev. Mol. Cell Biol.* **20**, 738–752 (2019).
8. P. K. Mattila, P. Lappalainen, Filopodia: Molecular architecture and cellular functions. *Nat. Rev. Mol. Cell Biol.* **9**, 446–454 (2008).
9. H. Elliott *et al*., Myosin II controls cellular branching morphogenesis and migration in three dimensions by minimizing cell-surface curvature. *Nat. Cell Biol.* **17**, 137–147 (2015).
10. R. S. Fischer, M. Gardel, X. Ma, R. S. Adelstein, C. M. Waterman, Local cortical tension by myosin II guides 3D endothelial cell branching. *Curr. Biol.* **19**, 260–265 (2009).
11. N. O. Alieva *et al*., Myosin IIA and formin dependent mechanosensitivity of filopodia adhesion. *Nat. Commun.* **10**, 3593 (2019).
12. C. G. Fonseca, P. Barbacena, C. A. Franco, Endothelial cells on the move: Dynamics in vascular morphogenesis and disease. *Vasc. Biol.* **2**, H29–H43 (2020).
13. B. Laviña *et al*., Defective endothelial cell migration in the absence of Cdc42 leads to capillary-venous malformations. *Development* **145**, dev161182 (2018).
14. A. Fantin *et al*., NRP1 regulates CDC42 activation to promote filopodia formation in endothelial tip cells. *Cell Rep.* **11**, 1577–1590 (2015). Correction in: *Cell Rep.* **13**, 2037 (2015).
15. N. Nohata *et al*., Temporal-specific roles of Rac1 during vascular development and retinal angiogenesis. *Dev. Biol.* **411**, 183–194 (2016).
16. C. A. Franco *et al*., SRF selectively controls tip cell invasive behavior in angiogenesis. *Development* **140**, 2321–2333 (2013).
17. C. Weinl *et al*., Endothelial SRF/MRTF ablation causes vascular disease phenotypes in murine retinae. *J. Clin. Invest.* **123**, 2193–2206 (2013).
18. C. A. Franco *et al*., Serum response factor is required for sprouting angiogenesis and vascular integrity. *Dev. Cell* **15**, 448–461 (2008).
19. H. Park *et al*., Integrin-linked kinase controls retinal angiogenesis and is linked to Wnt signaling and exudative vitreoretinopathy. *Nat. Commun.* **10**, 5243 (2019).
20. H. Yamamoto *et al*., Integrin β1 controls VE-cadherin localization and blood vessel stability. *Nat. Commun.* **6**, 6429 (2015).
21. L.-K. Phng, F. Stanchi, H. Gerhardt, Filopodia are dispensable for endothelial tip cell guidance. *Development* **140**, 4031–4040 (2013).
22. M. Vanlandewijck *et al*., A molecular atlas of cell types and zonation in the brain vasculature. *Nature* **554**, 475–480 (2018). Correction in: *Nature* **560**, E3 (2018).
23. A. Wang *et al*., Nonmuscle myosin II isoform and domain specificity during early mouse development. *Proc. Natl. Acad. Sci. U.S.A.* **107**, 14645–14650 (2010).
24. S. Claxton *et al*., Efficient, inducible Cre-recombinase activation in vascular endothelium. *Genesis* **46**, 74–80 (2008).
25. S. Even-Ram *et al*., Myosin IIA regulates cell motility and actomyosin-microtubule crosstalk. *Nat. Cell Biol.* **9**, 299–309 (2007). Correction in: *Nat. Cell Biol.* **9**, 480 (2007).
26. J. C. Sandquist, A. R. Means, The C-terminal tail region of nonmuscle myosin II directs isoform-specific distribution in migrating cells. *Mol. Biol. Cell* **19**, 5156–5167 (2008).
27. M. Vicente-Manzanares, M. A. Koach, L. Whitmore, M. L. Lamers, A. F. Horwitz, Segregation and activation of myosin IIB creates a rear in migrating cells. *J. Cell Biol.* **183**, 543–554 (2008).
28. S. Sawamiphak, M. Ritter, A. Acker-Palmer, Preparation of retinal explant cultures to study ex vivo tip endothelial cell responses. *Nat. Protoc.* **5**, 1659–1665 (2010).
29. C. Prahst *et al*., Mouse retinal cell behaviour in space and time using light sheet fluorescence microscopy. *eLife* **9**, e49779 (2020).
30. D. Krndija *et al*., Active cell migration is critical for steady-state epithelial turnover in the gut. *Science* **365**, 705–710 (2019).
31. E. T. Bishop *et al*., An in vitro model of angiogenesis: Basic features. *Angiogenesis* **3**, 335–344 (1999).
32. G. Guntas *et al*., Engineering an improved light-induced dimer (iLID) for controlling the localization and activity of signaling proteins. *Proc. Natl. Acad. Sci. U.S.A.* **112**, 112–117 (2015).
33. R. G. Hodge, A. J. Ridley, Regulating Rho GTPases and their regulators. *Nat. Rev. Mol. Cell Biol.* **17**, 496–510 (2016).
34. S. Etienne-Manneville, A. Hall, Integrin-mediated activation of Cdc42 controls cell polarity in migrating astrocytes through PKCzeta. *Cell* **106**, 489–498 (2001).
35. M. Chrzanowska-Wodnicka, K. Burridge, Rho-stimulated contractility drives the formation of stress fibers and focal adhesions. *J. Cell Biol.* **133**, 1403–1415 (1996).

36. J.-C. Kuo, X. Han, C.-T. Hsiao, J. R. Yates III, C. M. Waterman, Analysis of the myosin-II-responsive focal adhesion proteome reveals a role for β-Pix in negative regulation of focal adhesion maturation. *Nat. Cell Biol.* **13**, 383–393 (2011).
37. S. Huveneers, E. H. J. Danen, Adhesion signaling–Crosstalk between integrins, Src and Rho. *J. Cell Sci.* **122**, 1059–1069 (2009).
38. J. D. Rotty *et al*., Profilin-1 serves as a gatekeeper for actin assembly by Arp2/3-dependent and -independent pathways. *Dev. Cell* **32**, 54–67 (2015).
39. C. Suarez *et al*., Profilin regulates F-actin network homeostasis by favoring formin over Arp2/3 complex. *Dev. Cell* **32**, 43–53 (2015).
40. X. Ma *et al*., Nonmuscle myosin 2 regulates cortical stability during sprouting angiogenesis. *Mol. Biol. Cell* **31**, 1974–1987 (2020).
41. M.-F. Carlier, S. Shekhar, Global treadmilling coordinates actin turnover and controls the size of actin networks. *Nat. Rev. Mol. Cell Biol.* **18**, 389–401 (2017).
42. C. Léon *et al*., Megakaryocyte-restricted MYH9 inactivation dramatically affects hemostasis while preserving platelet aggregation and secretion. *Blood* **110**, 3183–3191 (2007).
43. A. N. Tullio *et al*., Nonmuscle myosin II-B is required for normal development of the mouse heart. *Proc. Natl. Acad. Sci. U.S.A.* **94**, 12407–12412 (1997).
44. J. Riedl *et al*., Lifeact mice for studying F-actin dynamics. *Nat. Methods* **7**, 168–169 (2010).
45. M. D. Muzumdar, B. Tasic, K. Miyamichi, L. Li, L. Luo, A global double-fluorescent Cre reporter mouse. *Genesis* **45**, 593–605 (2007).
46. Y. Zhang *et al*., Mouse models of MYH9-related disease: Mutations in nonmuscle myosin II-A. *Blood* **119**, 238–250 (2012).
47. C. A. Franco *et al*., Non-canonical Wnt signalling modulates the endothelial shear stress flow sensor in vascular remodelling. *eLife* **5**, e07727 (2016).